HOMOGENISATION AND NUMERICAL SIMULATION OF FLOW IN GEOMETRIES WITH TEXTILE MICROSTRUCTURES

M. GRIEBEL* AND M. KLITZ†

Abstract. The simulation of the Liquid Composite Moulding process is an important step for the manufacturing of composites with textile reinforcements. However, its fast direct numerical simulation is impossible on the microscale due to computational complexity reasons. We have to resort to the macroscale instead. Here, an essential task is the fast and accurate prediction of the permeability of textile microstructures. For textiles composed of impermeable yarns, we discuss the homogenisation of the Stokes equations. This leads to Darcy's law on the macroscale and gives the permeability via the so-called unit cell problems. These equations are then discretised and solved numerically. For textiles composed of permeable yarns, their dual porosity is accounted for by a fictitious domain approach in form of the Stokes/Brinkman equations. The results of our permeability computations in textiles are validated and compared to experimental data.

Key words. Homogenisation, multiscale porous media flow, permeability, textile composites

AMS subject classifications. 76S05, 35B27

1. Introduction. New materials with textile microstructures are used in an increasing number of industrial high-performance products such as aerospace components, boat hulls or racing car bodies since they combine strength and stiffness with lightness and corrosion-resistance. To manufacture these composite materials, Liquid Composite Moulding is employed, which comprises of a family of processes for the injection of resin into a closed cavity filled with fibre preforms. During the injection stage, the fabric conforms to the mould and is subjected to deformation and distortion which cause the individual fibre layers to nest, bend and shear. Here, the local permeability values of the preform differ significantly. These local changes in the permeability influence the formation of voids and bubbles, the degree of infiltration and the injection time. Therefore, the computation of the permeability and its changes due to bending, shearing, or nesting is a vital step in the design of the Liquid Composite Moulding process [30].

For the permeability prediction of fabric preforms, we must describe their geometric structure. To this end, we use the WiseTex [31] and LamTex [18] software. A representation of a textile geometry is shown in Figure 1.1 at different levels of resolution: On the microscale the fabric consists of individual strands of fibres (a). On the next coarser scale the fibres are bundled into tows or yarns (b), which are woven or stitched together to form an interconnected fabric network (c). In many cases the textile consists of periodic patterns of interlaced yarns or tows and can thus be conveniently described by repeated unit cells. The mould is then completely filled with fabric, i.e. covered with repeated unit cells (d). Altogether, the geometry of a fabric involves at least one microscale.

For the computation of permeability, we have to face the following two situations: If the yarns are impermeable, the resin infiltrating a fabric like the one shown in Figure 1.1 flows through the empty pores and channels of the fabric. In this case, the homogenisation of the Stokes equations yields Darcy's law on the macroscale. On the other hand, if the fabric's tows or yarns are porous themselves, then the resin also flows within the yarn on the microscale. In this case, we account for the porosity of

*Institute for Numerical Simulation, University of Bonn (griebel@ins.uni-bonn.de).
†Institute for Numerical Simulation, University of Bonn (klitz@ins.uni-bonn.de).

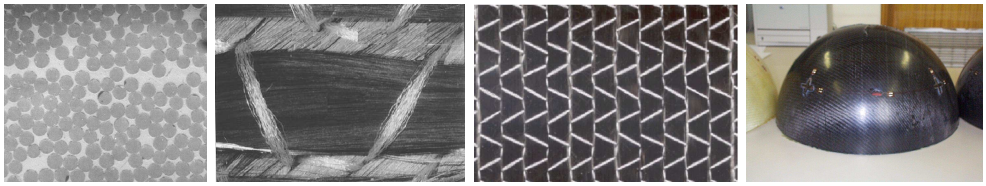

FIG. 1.1. *A hierarchy of textile structures from left to right: the fibres (a, 0.00001 m), the fabric unit cell (b, 0.01 m), the composite unit cell (c, 0.1 m), the composite part (d, 1 m) [Pictures by courtesy of S.V. Lomov].*

the textile on both scales by employing the so-called Stokes/Brinkman equations to predict the effective permeability of the fabric.

The contribution of this article is as follows. We use homogenisation to justify Darcy's law on the textile macroscale. In particular, we show that the computation of the permeability of a textile fabric defined by the solution of the unit cell problems in homogenisation theory is indeed equivalent to its computation by Darcy's law as e.g. done in [21] and in many other practical approaches to the subject. Furthermore, we discuss the validity of the Stokes/Brinkman equations which accounts for the dual porosity of textiles. We argue that, within the yarns, the Stokes/Brinkman equations reduce to Darcy's law and that their homogenisation yields a homogenised equation on the macroscale, which is again of Darcy type. As Mei, Auriault and Ng [19, p.295] point out: "There are many more theoretical papers applying the method of homogenization to a large variety of physical problems than there are quantitative solutions of the cell problems. The latter, however, is ultimately necessary to complete the scientific task." Indeed, we find that the theory of homogenisation is well accounted for in the literature (cf. [2, 13, 20, 25] and the references therein), but its numerical implementation and practical validation is scarce [15, 21, 24]. We therefore also discretise the derived equations with a finite volume method on a regular staggered grid and solve for the permeability. Then, we validate our numerical results against experimental data and show that we obtain good predictions for typical model problems. We furthermore apply our presented method to industrial textile reinforcements and give the corresponding permeability results.

The remainder of this article is organised as follows. In Section 2, we present the homogenisation of the Stokes equations and discuss the equivalence of different approaches for the computation of permeability for a numerical model problem. We then apply our approach to real industrial textiles composed of impermeable yarns and compare the computed permeability to experimental data. In Section 3, following [3], we discuss a dual porosity model for permeable yarns and present the fictitious domain method for the description of viscous flow in a single domain which embeds such yarns. The homogenisation of the resulting Stokes-Brinkman equations yields Darcy's law on the macroscale. For a numerical model problem, we show that the corresponding unit cell problem on the mesoscale approximates the Stokes unit cell problem on the microscale. Then, our dual porosity approach is applied to an industrial textile consisting of permeable yarns, and we compare the permeability of such a textile to experimental data.

2. Homogenisation of the Stokes equations in textile fabrics. In this section we show that the homogenisation of the Stokes equations, which describe the flow between solid yarn stacks in a periodically repeated textile cell on the mi-

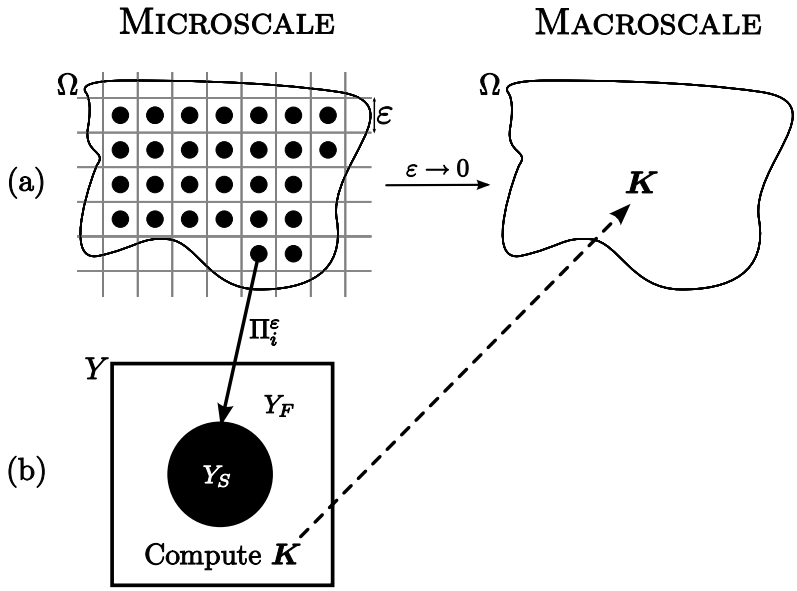

FIG. 2.1. *Sketch of the porous geometry Ω on the microscale and its unit cell Y. On the macroscale, the effective parameter $\boldsymbol{K}$ contains all information about the microscopic pore geometry.*

croscale, yields Darcy's law on the macroscale. Our interest in this is two-fold: On the one hand, there are a number of purely heuristic approaches, where filtration laws like Darcy's are successfully applied without any theoretical justification for the particular problem. On the other hand, in most literature on homogenisation theory [2, 13, 20, 25], porous media are considered which are composed of disconnected grains only. However, textile fabrics consist of connected yarn stacks. In the case of connected solid and fluid parts, homogenisation has been e.g. studied by Allaire [1] on a theoretical level so far. We show that textiles, which consist of connected solid and fluid parts, indeed fulfil the geometrical constraints in that work. See also [6] for the homogenisation in fibrous media which consist of layers of parallel fibres and compare the references to the scarce mathematical articles on fibrous porous media therein.

In practice, real-life textiles are significantly irregular due to the manufacturing process. Then, the multiple layers of textiles are most often nested and not arranged periodically. This may be accounted for by a homogenisation approach which includes stochastic variation of the geometry [7]. Nevertheless, in this article we assume an ideal periodic fabric, which principally consist of patterns of interlaced yarns or tows that repeat in the different directions.

2.1. Derivation of macroscopic equations. First, we require a mathematical description of admissible porous geometries. Throughout this article $\Omega \subset \mathbb{R}^3$ denotes an open, bounded and connected set with a smooth boundary of class C^1. Let $\varepsilon > 0$ and let the microscale be covered by a regular mesh of size ε. Each cell shall be denoted by $Y_i^\varepsilon =]0,\varepsilon[^3$ with $1 \leq i \leq N(\varepsilon)$, where $N(\varepsilon) = |\Omega|\varepsilon^{-3}(1+o(1))$ denotes the number of cells. Within each cell, we define the solid part $Y_{S_i}^\varepsilon$ which is also of the order ε. The fluid domain $\Omega_\varepsilon \subset \Omega$ is obtained from Ω by removing these periodically

distributed solid parts, i.e.

$$\Omega_\varepsilon = \Omega - \bigcup_{i=1}^{N(\varepsilon)} Y_{S_i}^\varepsilon. \tag{2.1}$$

Furthermore, we define the unit cell $Y =]0,1[^3$ by a linear homeomorphism Π_i^ε of each cell Y_i^ε with ratio of magnification $1/\varepsilon$, i.e. we rescale the cells Y_i^ε to one. Hence,

$$Y_S = \Pi_i^\varepsilon(Y_{S_i}^\varepsilon) \quad \text{and} \quad Y_F = \Pi_i^\varepsilon(Y_{F_i}^\varepsilon) \tag{2.2}$$

denote the solid and the fluid part of the unit cell. See Figure 2.1 for an example of a simple porous microgeometry. A textile unit cell is shown in Figure 2.2.

Next, we need a model for the fluid flow on the microscale between the yarns. For most flow problems in textiles on the microscale the advective inertial forces are small compared to the viscous forces. This flow behaviour is modelled by the incompressible Stokes equations

$$\left.\begin{aligned} \nabla p_\varepsilon - \mu\Delta \boldsymbol{u}_\varepsilon &= \boldsymbol{f} && \text{in } \Omega_\varepsilon \\ \nabla \cdot \boldsymbol{u}_\varepsilon &= 0 && \text{in } \Omega_\varepsilon \\ \boldsymbol{u}_\varepsilon &= 0 && \text{on } \partial\Omega_\varepsilon \end{aligned}\right\} \quad \mathcal{P}^\varepsilon, \tag{2.3}$$

where $\boldsymbol{u}_\varepsilon : \Omega_\varepsilon \to \mathbb{R}^3$ denotes the velocity field for the microscale geometry and $p_\varepsilon : \Omega_\varepsilon \to \mathbb{R}$ denotes the corresponding pressure.[1] Furthermore, $\boldsymbol{f}$ stands for volumetric forces such as gravity and μ denotes the viscosity.

In homogenisation theory the upscaled equation is obtained by letting the finer scale tend to zero. The basic idea behind this limit process is that the complicated microstructure averages out. To this end, one employs a multiscale expansion [20], which contains the behaviour of the fluid on the two different length scales $\boldsymbol{x}$ and $\boldsymbol{x}/\varepsilon$

$$\begin{aligned} \boldsymbol{u}_\varepsilon &= \varepsilon^2 \left\{ \boldsymbol{u}_0\left(\boldsymbol{x}, \frac{\boldsymbol{x}}{\varepsilon}\right) + \varepsilon \boldsymbol{u}_1\left(\boldsymbol{x}, \frac{\boldsymbol{x}}{\varepsilon}\right) + \varepsilon^2 \boldsymbol{u}_2\left(\boldsymbol{x}, \frac{\boldsymbol{x}}{\varepsilon}\right) + \ldots \right\} \\ p_\varepsilon &= \varepsilon^0 \left\{ p_0\left(\boldsymbol{x}, \frac{\boldsymbol{x}}{\varepsilon}\right) + \varepsilon p_1\left(\boldsymbol{x}, \frac{\boldsymbol{x}}{\varepsilon}\right) + \varepsilon^2 p_2\left(\boldsymbol{x}, \frac{\boldsymbol{x}}{\varepsilon}\right) + \ldots \right\}. \end{aligned} \tag{2.4}$$

Such an expansion for the velocity $\boldsymbol{u}_\varepsilon$ and the pressure p_ε is inserted into the fluid equations (2.3) on the microscale, along with similar transformations of the operators ∇ and Δ. In a next step, the limit $\lim_{\varepsilon\to 0} \boldsymbol{u}_\varepsilon$ is studied, which corresponds to letting the pore structure vanish. This is exemplified in Figure 2.1. For details on the homogenisation approach see [2, 13, 20, 25].

Note that equations (2.3) do not consist of a single Stokes problem, but of a whole series of problems $\mathcal{P}^\varepsilon$ when we let ε pass to zero. That is, the sequence of solutions $(\boldsymbol{u}_\varepsilon, p_\varepsilon)$ is not defined in a fixed domain independent of ε but in varying sets Ω_ε. However for homogenisation theory, convergence in fixed Sobolev spaces on Ω is required [27]. Therefore, we have to extend the velocity $\boldsymbol{u}_\varepsilon$ and the pressure p_ε from Ω_ε to the whole domain Ω by

$$\tilde{\boldsymbol{u}}_\varepsilon = \begin{cases} \boldsymbol{u}_\varepsilon & \text{in } \Omega_\varepsilon \\ 0 & \text{in } \Omega\backslash\Omega_\varepsilon \end{cases} \quad \text{and} \quad \tilde{p}_\varepsilon = \begin{cases} p_\varepsilon & \text{in } \Omega_\varepsilon \\ \frac{1}{\left|Y_{F_i}^\varepsilon\right|} \int_{Y_{F_i}^\varepsilon} p_\varepsilon \, d\boldsymbol{y} & \text{in } Y_{S_i}^\varepsilon \text{ for } 1 \le i \le N(\varepsilon). \end{cases} \tag{2.5}$$

[1] Note that the homogenisation of the Navier-Stokes equations yields different equations on the macroscale (e.g. Darcy's law, a nonlinear Navier-Stokes system with two pressures or ill-posed homogenised equations) depending on the influence of the nonlinear convective term [2, 20, 25]. However, if inertia effects are negligible, the formal asymptotic expansion again gives Darcy's law.

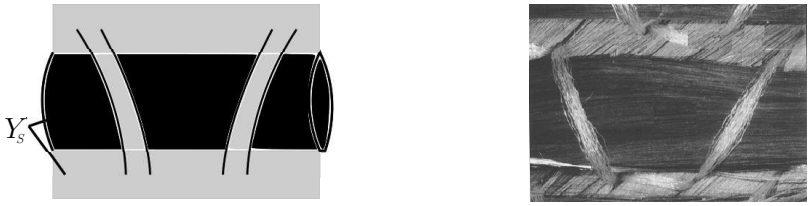

FIG. 2.2. *Example of a textile's fabric unit cell [Right picture by courtesy of S.V. Lomov].*

For simple geometries which are composed of disconnected grains that are entirely included in an ε-sized cell, Tartar [27] proved the existence of an extension for the pressure (2.5) which allows to pass from the Stokes equations $\mathcal{P}_\varepsilon$ to the limit problem of Darcy's law. However, textiles typically consist of connected solid and fluid parts. This more realistic case is studied by Allaire [1]. Furthermore, he also accounts for solid cells $Y_{S_i}^\varepsilon$ that are allowed to cut the boundary, which (in Theorem 2.1) restricts the pressure $\tilde{p}_\varepsilon$ to converge only locally in $L^2_{\mathrm{loc}}(\Omega)\backslash\mathbb{R}$.

To apply this approach in our context, we have to verify Allaire's assumptions on porous geometries for our textiles. To this end, we require some notational details. We denote by $E_S \subset \mathbb{R}^3$ the closed set that is obtained by Y-periodic repetition of Y_S in the entire space $\mathbb{R}^3$ and we denote its fluid counterpart by E_F. The following hypotheses have to be satisfied [1]:

i. Y_F and Y_S have strictly positive measures in $\bar{Y}$.
ii. E_F and the interior of E_S are open sets with C^1 boundaries and are locally located on one side of their boundary; furthermore E_F is connected.
iii. Y_F is an open set with a local Lipschitz boundary.

Let us consider the implications of these hypotheses for textiles in more detail. One elementary cell Y of a textile consists of both fabric and fluid parts as depicted in Figure 2.2. Therefore, assumption (i) is fulfilled. Furthermore, we assume that textiles consist of periodic repeat cells with the obstacles touching the boundary. Therefore, the solid part Y_S as well as the fluid part Y_F of the repeat cell must be Y-periodic and the repetitions of Y_S and Y_F in $\mathbb{R}^3$, i.e. E_F and E_S, must be fully connected. Thus, both have a C^1 boundary, and assumption (ii) is fulfilled. Furthermore, we assume that the boundary of Y_F is sufficiently regular so that (iii) holds.

Altogether, Allaire's requirements fit with the properties of textiles intended for LCM processes. Consequently, the following theorem holds for our periodically repeated textile fabrics. It states that the solutions $(\tilde{\boldsymbol{u}_\varepsilon}, \tilde{p_\varepsilon})$ converge to the solutions of Darcy's law for $\varepsilon \to 0$.

THEOREM 2.1 (Darcy's law). *Let the assumptions (i)-(iii) be fulfilled and let $(\boldsymbol{u}_\varepsilon, p_\varepsilon)$ denote the solution of the Stokes problem $\mathcal{P}^\varepsilon$. Then, $\tilde{\boldsymbol{u}}_\varepsilon/\varepsilon^2$ converges weakly in $L^2(\Omega)^3$ to $\boldsymbol{u}$, and $\tilde{p_\varepsilon}$ converges strongly in $L^2(\Omega)\backslash\mathbb{R}$ to p, where $(\boldsymbol{u}, p)$ is the solution of the homogenised problem*

$$\mathcal{P}^0 = \begin{cases} \boldsymbol{u} = \dfrac{1}{\mu}\boldsymbol{K}(\boldsymbol{f} - \nabla p) & \text{in } \Omega \\ \nabla \cdot \boldsymbol{u} = 0 & \text{in } \Omega \\ \boldsymbol{u} \cdot \boldsymbol{\nu} = 0 & \text{on } \partial\Omega, \end{cases} \tag{2.6}$$

and $\boldsymbol{\nu}$ is the unit normal. The permeability tensor $\boldsymbol{K} = K_{ij}$ is defined by

$$K_{ij} = \langle \nabla_y \boldsymbol{w}^i : \nabla_y \boldsymbol{w}^j \rangle_Y \tag{2.7}$$

for $1 \leq i,j \leq 3$, *where* $\langle \cdot \rangle_Y = \frac{1}{|Y|}\int_Y \cdot \, d\boldsymbol{y}$. *Here,* : *denotes the Frobenius inner product, and* $\boldsymbol{w}^i$ *denotes the solution of the cell problem: For* $1 \leq i,j \leq 3$ *find* $(\boldsymbol{w}^i, \pi^i) \in H^1(Y_F)^3 \times L^2(Y_F)\backslash\mathbb{R}$ *such that*

$$\begin{aligned} -\Delta \boldsymbol{w}^i + \nabla \pi^i &= \boldsymbol{e}^i \quad \text{in } Y_F \\ \nabla \cdot \boldsymbol{w}^i &= 0 \quad \text{in } Y_F \\ \boldsymbol{w}^i &= 0 \quad \text{on } \partial Y_S \\ \boldsymbol{w}^i, \pi^i & \quad Y-\text{periodic}, \end{aligned} \tag{2.8}$$

where $\boldsymbol{e}^i$ *is the vector with components* $e^i_j = \delta_{ij}$.

Proof. See Allaire [1]. □

Note that it can be shown that $\boldsymbol{K}$ is symmetric and positive definite and that there holds the equation

$$\langle \nabla_y \boldsymbol{w}^i : \nabla_y \boldsymbol{w}^j \rangle_Y = \langle w^i_j \rangle_Y, \tag{2.9}$$

where w^i_j denotes the j-th component of $\boldsymbol{w}^i$ for $1 \leq i,j \leq 3$, [25]. This allows for a simplified computation of the permeability tensor $\boldsymbol{K}$.

2.2. Permeability computation. In this subsection we show that the computation of the permeability $\boldsymbol{K}$ by the unit cell problems is equivalent to the solution of the Stokes equations and the subsequent insertion of $\boldsymbol{u}^i_\varepsilon$ and p^i_ε into Darcy's law. Here, the Stokes equations have to be solved three times in the repeat cell Y^ε of the porous medium, i.e. for $1 \leq i \leq 3$, we have to find $\{\boldsymbol{u}^i_\varepsilon, p^i_\varepsilon\}$ such that

$$\begin{aligned} \nabla p^i_\varepsilon - \mu \Delta \boldsymbol{u}^i_\varepsilon &= \boldsymbol{f}^i \quad \text{in } Y^\varepsilon_F \\ \nabla \cdot \boldsymbol{u}^i_\varepsilon &= 0 \quad \text{in } Y^\varepsilon_F \\ \boldsymbol{u}^i_\varepsilon &= 0 \quad \text{on } \partial Y^\varepsilon_S \\ \boldsymbol{u}^i_\varepsilon, p^i_\varepsilon & \quad Y^\varepsilon\text{-periodic}. \end{aligned} \tag{2.10}$$

Then, for $1 \leq j \leq 3$, we insert $\{\boldsymbol{u}^i_\varepsilon, p^i_\varepsilon\}$ into Darcy's law. This results in

$$\left\langle u^i_{\varepsilon,j} \right\rangle_{Y_\varepsilon} = \frac{1}{\mu} \sum_{k=1}^{3} K_{jk} \left(f^i_k - \left\langle \frac{\partial p^i_\varepsilon}{\partial x_k} \right\rangle_{Y_\varepsilon} \right), \tag{2.11}$$

where $u^i_{\varepsilon,j}$ now denotes the j-th component of the vector $\boldsymbol{u}^i_\varepsilon$. Note here that the average pressure drop vanishes since the pressure is periodic, i.e.

$$\left\langle \frac{\partial p^i_\varepsilon}{\partial x_k} \right\rangle_{Y_\varepsilon} = 0.$$

Note furthermore that the permeability is an *intrinsic property of the geometry.* Therefore, $\boldsymbol{K}$ neither depends on the force $\boldsymbol{f}$ nor on the viscosity μ of (2.10). Thus, we may choose $f^i_k = \delta_{ik}$ and $\mu = 1$ in (2.11) which yields

$$K_{ij} = K_{ji} = \left\langle u^i_{\varepsilon,j} \right\rangle_{Y_\varepsilon}. \tag{2.12}$$

Since the permeability depends on the geometry only, we are also allowed to rescale the size of the repeat cell Y^ε to one as in (2.2). With this in mind, a comparison

of the above computation of permeability by equations (2.10) and (2.12) with the solution of the unit cell problems (2.8) and the subsequent definition of permeability (2.9) shows that both approaches are indeed the same.

Alternatively, in many practical experiments a pressure drop $(\delta p)_i$ is applied as the driving force in the Stokes equations (2.10). The pressure p_ε^i can then be subdivided into a periodic and a linear varying part

$$p_\varepsilon^i = \hat{p}_\varepsilon^i + (\delta p)_i.$$

Again, since $\boldsymbol{K}$ is independent of the magnitude of the pressure drop, we may choose $(\delta p)_i = -x_i$ so that

$$\nabla p_\varepsilon^i = \nabla \hat{p}_\varepsilon^i - \boldsymbol{e}_i.$$

Then, the first equation in (2.10) reads as

$$\nabla \hat{p}_\varepsilon^i - \mu \Delta \boldsymbol{u}_\varepsilon^i = \boldsymbol{e}_i.$$

If we now insert the solution of the Stokes equations into Darcy's law, the permeability can again be computed by (2.12).

We conclude that there are now two equivalent approaches for the computation of $\boldsymbol{K}$:

(a) By Darcy's law from a prior solution of the Stokes equations (with a volume force or an applied pressure gradient).
(b) From the unit cell problems (2.8).

In the following, we discuss the numerical implementation of both approaches and compute $\boldsymbol{K}$ for a simple test problem. We then apply approach (a) for the permeability computation of industrial textiles from real-life applications.

2.3. Numerical treatment of Darcy's law and the unit cell problems. Both the numerical solution of the unit cell problems (2.8) and the computation of the permeability by Darcy's law (2.12) involve the solution of the Stokes equations. As a basis for our implementation, we use the three-dimensional instationary Navier-Stokes solver NaSt3DGP developed at the Institute for Numerical Simulation at the University of Bonn [10]. Here, we solve the Stokes equations numerically on a regular staggered grid with a finite volume discretisation. NaSt3DGP employs a Chorin projection method. Moreover, we use a pseudo time-stepping technique to advance to the steady state. For this, we discretise the Stokes equations implicitly in time by a Crank-Nicolson scheme.

Note that we also experimented with the full Navier-Stokes equations for the computation of permeability. However, for our textile applications, the convective term was extremely small and hence could be neglected. Also, a direct Stokes solver without pseudo time-stepping has been recently implemented for the considered textile geometries [28, 29].

In the following, we always compute K_{11} only. Therefore, we skip the upper index of the velocity components and write $\boldsymbol{w^1} = (w_i)_{i=1,\ldots,3}$ and $\boldsymbol{u^1} = (u_i)_{i=1,\ldots,3}$.

2.3.1. Test problem: 3D array of spheres. As a simple first example, we compare our numerical permeability computations with semi-analytical results for a porous medium which consists of cubic arrays of spheres. Note that such beds of spheres are employed in the numerical simulation of filters, catalytic packs or heat exchangers. This setup is by far not adequate for actual textile permeability problems,

TABLE 2.1
Convergence table for the computation of permeability K_{11} in a 3D array of spheres with radii $r = 0.1$, $r = 0.2$ and $r = 0.3$.

Cells	K_{11} for $r = 0.1$	K_{11} for $r = 0.2$	K_{11} for $r = 0.3$
32^3	3.9528_{-1}	1.2473_{-1}	4.5216_{-2}
64^3	3.8447_{-1}	1.2330_{-1}	4.4667_{-2}
128^3	3.8213_{-1}	1.2292_{-1}	4.4437_{-2}

TABLE 2.2
Computation of the permeability K_{11} in a 3D array of spheres for different radii r and comparison to semi-analytical results from [26].

Cells	r	K_{11} Darcy	K_{11} Cell	K_{11} [26]	Abs. err.	Rel. err
64^3	0.10	3.8447_{-1}	3.8447_{-1}	3.8219_{-1}	2.28_{-3}	0.60%
64^3	0.15	2.0926_{-1}	2.0926_{-1}	2.0805_{-1}	1.21_{-3}	0.58%
64^3	0.20	1.2330_{-1}	1.2330_{-1}	1.2327_{-1}	3.00_{-5}	0.02%
64^3	0.25	7.4091_{-2}	7.4091_{-2}	7.4668_{-2}	5.77_{-4}	0.77%
64^3	0.30	4.4667_{-2}	4.4667_{-2}	4.4501_{-2}	1.66_{-4}	0.37%
64^3	0.35	2.5216_{-2}	2.5216_{-2}	2.5246_{-2}	3.00_{-5}	0.12%

which will be considered later in Subsections 2.4 and 3.7 in more detail. It merely serves to show the basic properties of our numerical homogenisation approach. Here, the permeability tensor takes the form $\boldsymbol{K} = K_{11}\boldsymbol{I}$ for the isotropic sphere with $\boldsymbol{I}$ the unit matrix, i.e. we only need to compute K_{11}.

As a first step we compute the permeability by the unit cell problems on successively refined grids for sphere radii $r = 0.1$, 0.2 and 0.3. Results are shown in Table 2.1. Furthermore, we compute the grid convergence rate

$$\rho(r) = \ln\left(\frac{\|w_{1,2h} - w_{1,4h}\|_{l^1_{2h}}}{\|w_{1,h} - w_{1,2h}\|_{l^1_h}}\right) / \ln 2$$

of the velocity component w_1 in the flow direction. Here, $\|\cdot\|_{l^1_h}$ denotes the discrete l_1-norm evaluated on the grid with mesh size h. The subscripts h, $2h$ and $4h$ denote solutions or evaluations on grids with mesh sizes h, $2h$ and $4h$, respectively.[2] We obtained $\rho(0.3)$=1.26, $\rho(0.2)$=1.86 and $\rho(0.1)$=2.21, i.e. the order of convergence improves with smaller sphere size. This is to be expected since a larger sphere means more boundary cells, which are approximated to first order only.

In the same setup, Sangani and Acrivos [26] found general solutions of the Stokes equations as a series formulation, whose coefficients were determined numerically. The authors computed the dimensionless drag force F to which the first entry of the permeability tensor is related by $K_{11} = \frac{1}{6}\pi r F$. We solve both the unit cell problems and the Stokes equations as input for Darcy's law for the computation of the permeability. These steady state numerical results, as well as the semi-analytical ones, are given in Table 2.2 for different sphere radii.[3]

[2]The time step in our instationary solver is restricted by that on the finest mesh. Here, we stop the computation when $\left\|w^{n+1}_{1,h} - w^n_{1,h}\right\|_{l^1_h} \leq 1_{-10}$, i.e. the difference between the velocity component w_1 of two successive time steps falls below the threshold 1_{-10}.

[3]Note that in [26], instead of the radius, scaled sphere volume fractions $\chi = (V_f/V_{f\max})^{1/3}$ are used. In an arbitrary single cell of length L, the volume fraction $V_f = 4\pi r^3/3L^3$ denotes the total

TABLE 2.3
Permeability results for the Monofilament Fabric Natte 2115 with one layer and two layers with minimal and maximal nesting. $L = (L_x, L_y, L_z)$ denotes the length of the fabric unit cell.

Model	L_x (mm)	L_y (mm)	L_z (mm)	Resolution	K_{xx} (mm^2)
Single-layer	2.26	2.16	0.4	$226 \times 216 \times 40$	3.289_{-4}
Minimum nesting	2.26	2.16	0.8	$226 \times 216 \times 80$	3.289_{-4}
Maximum nesting	2.26	2.16	0.78	$226 \times 216 \times 78$	2.023_{-4}

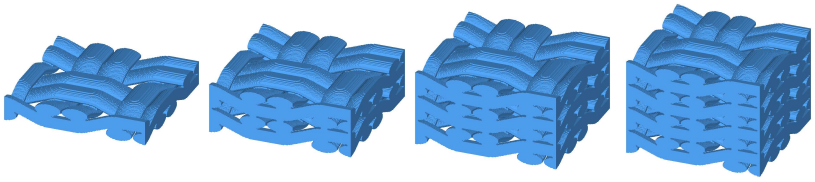

FIG. 2.3. *Non-nested layering of the Monofilament Fabric Natte 2115.*

We see from Table 2.2 that the computation of the permeability K_{11} by the unit cell problems is indeed equivalent to the solution of the Stokes equations and the subsequent insertion of $\boldsymbol{u}_\varepsilon^1$ and p_ε^1 into Darcy's law, i.e. both methods give the same results for K_{11}. Furthermore, we observe that all computed values are in good agreement with those obtained analytically by Sangani and Acrivos [26]. They deviate no more than 0.8%. Note that the permeabilities given in Table 2.1 do not converge to the semi-analytical values. This cannot be expected anyway, since the semi-analytical results rely on analytical as well as on numerical approximations themselves.

2.4. Computation of textile permeability. Now, we apply our approach to real industrial textiles which consist of impermeable yarns. A key task in permeability modelling is the geometric description of textile structures which will result in the reinforcement of the composite material after the LCM process. The basic geometric structure of a textile can be described by a single layer model for which we employ the WiseTex software [31] developed at the Katholieke Universiteit Leuven in Belgium. More complex textile structures, however, are multi-layered and the different layers are 'nested'. Building the geometry model of a multi-layered reinforcement is an additional step, for which we use the LamTex software [18]. An example is given in Figure 2.3 and Figure 2.4. Figure 2.3 shows successively stacked layers which are just simple repetitions of the first layer. However, in real-life textiles, neighbouring fabric layers further interact due to e.g. compression and other outer forces. Then the multiple layers tend to nest and no longer form a direct repetition of the single layer. Thus, a norm cell with more than just one single layer is to be employed. This also resembles the experimental setup. An example is given in Figure 2.4, where a non-nested and a maximally nested two-layer cell are shown, i.e. a cell for which the two layers fit maximally into each other. In laboratory experiments the layers even involve random nesting since they are randomly compressed in the mould cavity due to fabrication pressure and other outer forces. In the following, we use approach (a) of Section (2.2), i.e. we first solve the Stokes equations and then Darcy's law for the computation of $\boldsymbol{K}$.

As a typical example we consider the Monofilament Fabric Natte 2115. It

fraction of the cell that is occupied by the solid. Furthermore, $V_{f\max} = \pi/6$ corresponds to the case when the spheres are in contact. Since we solve the problems in a unit cell, there holds $\chi = 2r$.

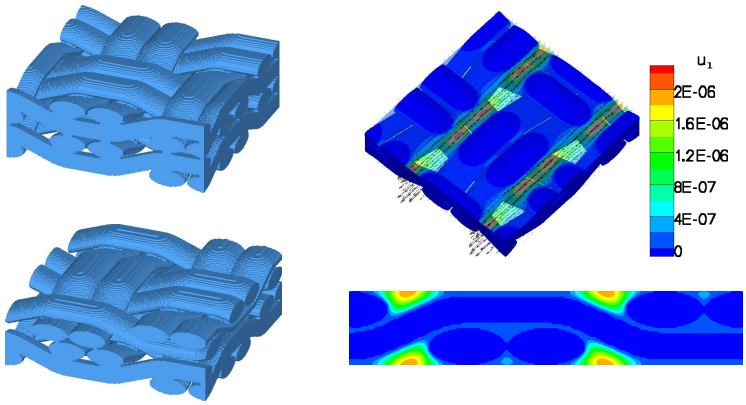

FIG. 2.4. *Two layers of the Monofilament Fabric Natte 2115; left: no nesting (top) and maximum nesting (bottom) discretised with grid cell size 0.01; right: 3D flow field and its 2D cut calculated in the fabric.*

is made of interwoven strands of PVC coated glass fibres, which are heated after the impregnation process so that the PVC coating melts and crossing yarns are fused together. This fabric is depicted in Figure 2.4. Natte 2115 is an ideal test fabric for permeability measurements on actual textile reinforcements in the laboratory. It consists of impermeable yarns, it is stable and reusable and it has many useful properties for permeability validation [28]. The full description of the Monofilament Fabric Natte 2115 can be found in [11, 12].

For our numerical calculations, we discretise the textile model with a very high resolution of $\Delta x = \Delta y = \Delta z = 0.01$. Then, according to approach (a), we solve the Stokes equations in a unit cell and insert the resulting velocity and pressure into Darcy's Law to obtain $\boldsymbol{K}$. The computed flow field of the velocity component u_1 is shown in Figure 2.4 together with a 2D cut, which displays the textile geometry and the flow between the yarns.

Table 2.3 shows the computed permeability K_{11} of the x-direction for different nesting structures of the Natte 2115. Here, we consider a one- and a two-layer cell with varying degrees of nesting. First of all, both the permeability computations for one layer and for two layers with minimum nesting give the same results. In this case, the second layer is a simple repetition of the first. Therefore the same result is to be expected and reflects our periodicity assumption on the textile structure. Second, if the layers are maximally nested, less fluid flows through the textile and, accordingly, the permeability decreases.

Note that practical experiments and measurements are usually performed with several layers of the Natte 2115 to fit to the laboratory setup: The layers are compressed in the mould cavity. This leads to a random variety of degrees of nesting including maximally nested parts which prevent fluid flow through the textile. As a result, any measured experimental permeability must be lower than that for the purely non-nested case. As a first approximation to this situation, we computed an average permeability between minimum and maximum nesting. The obtained value was 2.656_{-4}mm^2. Note that this averaged value and the experimentally obtained value of $2.7_{-4}\,\text{mm}^2 \pm 10\,\%$ coincide quite well. Nevertheless, further computations involving random nesting are necessary to confirm this result since permeability does

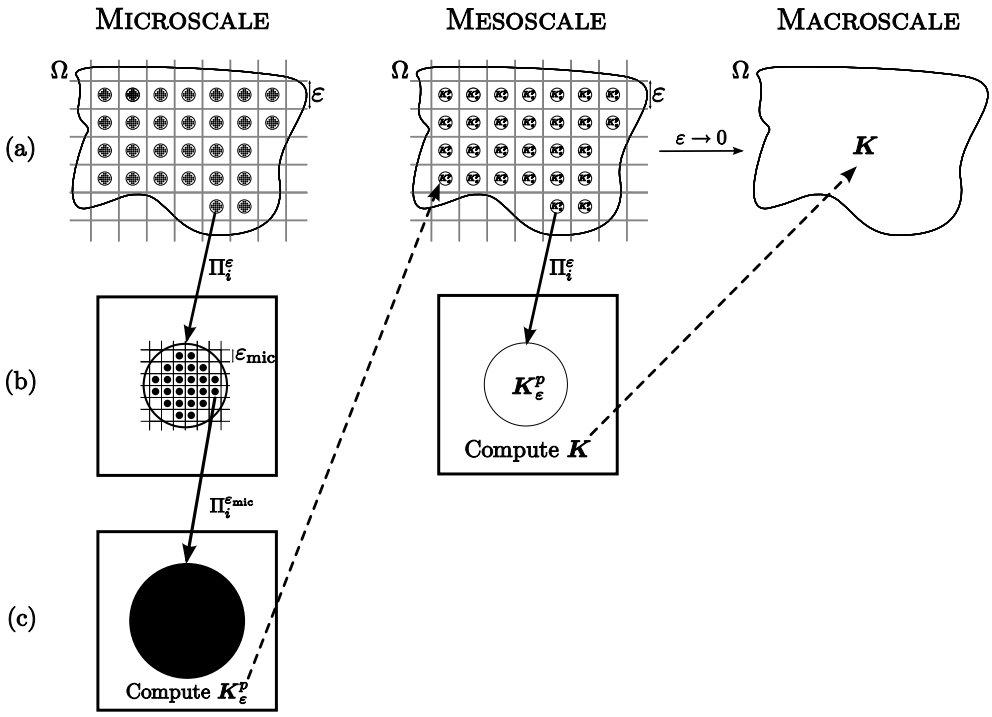

FIG. 3.1. *Sketch of a dually porous geometry* Ω. *On the microscale it contains porous obstacles and therefore has two unit cells. On the mesoscale, the geometric information about the porous obstacles is contained in the effective parameter* $\boldsymbol{K}_\varepsilon^p$. *Here, we solve the Brinkman unit cell problems (3.10) for the computation of* $\boldsymbol{K}$ *for Darcy's law on the macroscale.*

not depend linearly on the volume fraction; see also [28].

3. Coupled Flow Problems in Plain and Porous Media. So far we considered the case of solid yarn stacks. We now turn to porous yarns, where flow also takes place inside the yarns. Thus, we consider domains $\Omega_\varepsilon = \Omega_\varepsilon^f \cup \Lambda_\varepsilon \cup \Omega_\varepsilon^p$, where Ω_ε^f still denotes the pure fluid domain which now embeds porous obstacles Ω_ε^p (cf. Figure 3.1). The regular hypersurface Λ_ε separates the fluid and the porous domain. Now, we have to additionally model the flow in the porous obstacles by e.g. the Darcy or Brinkman equations in Ω_ε^p, and we further have to couple this model with the Stokes equations in the fluid domain Ω_ε^f.

In this section, we shortly discuss coupling conditions which are formulated on the mesoscale; see Figure 3.1. Then, we propose the Stokes/Brinkman model as a single system of partial differential equations in both Ω_ε^f and Ω_ε^p. The error between this unified approach and a coupling approach with explicit interface conditions can be estimated [3]. We extend this estimate to non-scalar permeabilities. Furthermore, we present the homogenisation of the Stokes/Brinkman equations on the mesoscale, which yields Darcy's law on the macroscale and a further set of unit cell problems for the computation of $\boldsymbol{K}$.

3.1. Explicit interface conditions. Suppose that flow in the porous obstacles Ω_ε^p is modelled by Darcy's law

$$\begin{aligned} \boldsymbol{u}_\varepsilon^p &= -\frac{\boldsymbol{K}_\varepsilon}{\mu}\left(\nabla p_\varepsilon^p - \boldsymbol{f}^p\right) \\ \nabla \cdot \boldsymbol{u}_\varepsilon^p &= 0, \end{aligned} \tag{3.1}$$

and the flow in Ω_ε^f is modelled by the Stokes equations

$$\begin{aligned} -\mu\Delta \boldsymbol{u}_\varepsilon^f + \nabla p_\varepsilon^f &= \boldsymbol{f}^f \\ \nabla \cdot \boldsymbol{u}_\varepsilon^f &= 0. \end{aligned} \tag{3.2}$$

The coupling of these two systems is mathematically difficult, since the Stokes equations and Darcy's law are PDEs of different order and thus need a different number of conditions on their common interface.[4] If instead the flow in the porous obstacles is modelled by the Brinkman equation in Ω_ε^p

$$\begin{aligned} -\tilde{\mu}\Delta \boldsymbol{u}_\varepsilon^p + \nabla p_\varepsilon^p + \mu \boldsymbol{K}_\varepsilon^{-1}\boldsymbol{u}_\varepsilon^p &= \boldsymbol{f}_p \\ \nabla \cdot \boldsymbol{u}_\varepsilon^p &= 0, \end{aligned} \tag{3.3}$$

the coupling with the Stokes equations is more straightforward, since both equations are PDEs of the same order.[5] One possibility for their coupling are the transmission conditions

$$\boldsymbol{u}_\varepsilon^f|_{\Lambda_\varepsilon} = \boldsymbol{u}_\varepsilon^p|_{\Lambda_\varepsilon} \text{ and } \left(-p_\varepsilon^f \boldsymbol{I} + \mu\nabla \boldsymbol{u}_\varepsilon^f\right)\cdot\boldsymbol{\nu}|_{\Lambda_\varepsilon} = \left(-p_\varepsilon^p \boldsymbol{I} + \mu\nabla \boldsymbol{u}_\varepsilon^p\right)\cdot\boldsymbol{\nu}|_{\Lambda_\varepsilon} \tag{3.4}$$

on the interface Λ_ε, where again $\boldsymbol{\nu}$ denotes the unit normal. In the next step, we reformulate this approach as a single system of partial differential equations for the flow both in the pure fluid and in the porous domain.

3.2. The Stokes/Brinkman equations. The coupled Stokes/Brinkman equations are given by

$$\begin{aligned} -\tilde{\mu}\Delta \boldsymbol{u}_\varepsilon + \nabla p_\varepsilon + \mu \boldsymbol{K}_\varepsilon^{-1}\boldsymbol{u}_\varepsilon &= \boldsymbol{f} \quad && \text{in } \Omega_\varepsilon \\ \nabla \cdot \boldsymbol{u}_\varepsilon &= 0 && \text{in } \Omega_\varepsilon \\ \boldsymbol{u}_\varepsilon &= 0 && \text{on } \partial\Omega_\varepsilon, \end{aligned} \tag{3.5}$$

where $\boldsymbol{K}_\varepsilon$ is a positive definite diagonal tensor and $\tilde{\mu} > 0$ denotes an effective Brinkman viscosity. Here, the different parts of the domain are taken into account by their characteristic permeability, which has a finite value for the porous domain and an infinite value for the pure fluid domain. In addition, the viscosity may vary from its specific value in the pure fluid domain to some effective value in the porous part.

To be precise, we set

$$\boldsymbol{K}_\varepsilon = \begin{cases} \infty & \text{in } \Omega_\varepsilon^f \\ \boldsymbol{K}_\varepsilon^p & \text{in } \Omega_\varepsilon^p. \end{cases} \quad \text{and} \quad \tilde{\mu} = \mu \text{ in } \Omega_\varepsilon$$

[4] To this end, the Beavers-Joseph condition for the velocity may be employed. This can be experimentally and mathematically justified (cf. [5, 15, 20, 23] and the references cited therein).

[5] Note that a Brinkman type equation similar to (3.3) can be derived by homogenisation theory if, in contrast to Section 2, we assume that the obstacle size passes faster to zero than the inter-obstacle distance ε. The resulting equation is then valid for very low porosities only; cf. [14, 15] and the references cited therein.

Then, in the fluid region Ω_ε^f, this selection of parameters implies that equations (3.5) reduce to the Stokes equations (3.2). In the porous region Ω_ε^p, we take $\boldsymbol{K}_\varepsilon = \boldsymbol{K}_\varepsilon^p$, i.e. the Darcy permeability of the porous medium. Then, the only difference between equation (3.5) and Darcy's law (3.1) is the additional term $\tilde{\mu}\Delta\boldsymbol{u}_\varepsilon$. Since typical textile permeabilities $\boldsymbol{K}_\varepsilon^p$ range from $10_{-4}\,\mathrm{mm}^2$ to $10_{-7}\,\mathrm{mm}^2$, the penalisation term $\mu\boldsymbol{K}_\varepsilon^{-1}\boldsymbol{u}_\varepsilon$ becomes very large. If we choose $\tilde{\mu} = \mu$, it dominates $\tilde{\mu}\Delta\boldsymbol{u}_\varepsilon$ by many orders, and thus we approximately solve Darcy's Law in the porous part Ω_ε^p.[6]

3.3. Error Estimate for the Stokes/Brinkman Equations. In [3] Angot proves an estimate for the error between the Stokes/Brinkman equations (3.5) and the explicitly coupled system of the Stokes equations (3.2) and the Brinkman equation (3.3 - 3.4). For this estimate a scalar permeability is assumed, since in the articles [3] and [4] fluid-solid configurations are of main interest, as opposed to the fluid-porous ones. For our applications, the anisotropic textile geometry has to be accounted for by a permeability in tensor form. In the following, we therefore extend Angot's estimate [3] to the case that $\boldsymbol{K}_\varepsilon^p$ is a positive definite diagonal matrix. Here, $\boldsymbol{V} = \{\boldsymbol{u} \in H_0^1(\Omega_\varepsilon)^3$ such that $\nabla \cdot \boldsymbol{u} = 0\}$ denotes the Hilbert space of divergence-free functions.

THEOREM 3.1 (Error estimate for the Stokes/Brinkman equations). *Let $\delta > 0$ be a given parameter and let $(\boldsymbol{u}_{\varepsilon,\delta}, p_{\varepsilon,\delta}) \in \boldsymbol{V} \times L^2(\Omega_\varepsilon)/\mathbb{R}$ denote the solution of the Stokes/Brinkman problem (3.5) over the whole fictitious domain Ω_ε with a positive definite diagonal second-order tensor $\boldsymbol{K}_\varepsilon$, where*

$$\boldsymbol{K}_\varepsilon|_{\Omega_f^\varepsilon} = \frac{1}{\delta}\boldsymbol{I}, \quad \boldsymbol{K}_\varepsilon|_{\Omega_\varepsilon^p} = \boldsymbol{K}_\varepsilon^p.$$

Furthermore, set $\tilde{\mu} = \mu$ in Ω_ε for the effective viscosity. Moreover, let $\boldsymbol{u}_\varepsilon$ be the solution of the fluid-porous transmission problem (3.2, 3.3, 3.4). Then, if $\boldsymbol{f} \in L^2(\Omega_\varepsilon)^3$ and if Ω_ε^f and Ω_ε^p are in C^2, the error estimate

$$||\boldsymbol{u}_{\varepsilon,\delta} - \boldsymbol{u}_\varepsilon||_{H^1(\Omega)} = \mathcal{O}(\delta) \tag{3.6}$$

holds for the solution $\{\boldsymbol{u}_{\varepsilon,\delta}\}_{\delta>0}$ of (3.5).

Proof. The case of a scalar K_ε^p is dealt with in [3]. Here, we just have to describe the necessary extensions for positive definite diagonal matrices $\boldsymbol{K}_\varepsilon^p$. The weak formulation of the Stokes/Brinkman problem (3.5) reads

$$\begin{aligned} &\mu \int_{\Omega_\varepsilon^f} \nabla\boldsymbol{u}_{\varepsilon,\delta} : \nabla\boldsymbol{\varphi}\, d\boldsymbol{x} + \tilde{\mu} \int_{\Omega_\varepsilon^p} \nabla\boldsymbol{u}_{\varepsilon,\delta} : \nabla\boldsymbol{\varphi}\, d\boldsymbol{x} \\ &+\mu\delta \int_{\Omega_\varepsilon^f} \boldsymbol{u}_{\varepsilon,\delta} \cdot \boldsymbol{\varphi}\, d\boldsymbol{x} + \mu \int_{\Omega_\varepsilon^p} (\boldsymbol{K}_\varepsilon^p)^{-1}\boldsymbol{u}_{\varepsilon,\delta} \cdot \boldsymbol{\varphi}\, d\boldsymbol{x} = \int_{\Omega_\varepsilon} \boldsymbol{f} \cdot \boldsymbol{\varphi}\, d\boldsymbol{x} \end{aligned} \tag{3.7}$$

for all $\boldsymbol{\varphi} \in \boldsymbol{V}$. Note that the pressure integral vanishes because $\boldsymbol{\varphi}$ is divergence-free in Ω. We denote the diagonal entries of $\boldsymbol{K}_\varepsilon^p$ by $(\kappa_i)_{i=1,\dots,3}$. Now, we choose $\boldsymbol{\varphi} = \boldsymbol{u}_{\varepsilon,\delta}$ and divide by $\mu > 0$. This results in

$$\begin{aligned} &\int_{\Omega_\varepsilon^f} |\nabla\boldsymbol{u}_{\varepsilon,\delta}|^2\, d\boldsymbol{x} + \frac{\tilde{\mu}}{\mu} \int_{\Omega_\varepsilon^p} |\nabla\boldsymbol{u}_{\varepsilon,\delta}|^2\, d\boldsymbol{x} \\ &+\delta \int_{\Omega_\varepsilon^f} |\boldsymbol{u}_{\varepsilon,\delta}|^2\, d\boldsymbol{x} + \int_{\Omega_\varepsilon^p} \sum_{i=1}^{3} \kappa_i^{-1} u_{\varepsilon,\delta,i}^2\, d\boldsymbol{x} = \frac{1}{\mu} \int_{\Omega_\varepsilon} \boldsymbol{f} \cdot \boldsymbol{u}_{\varepsilon,\delta}\, d\boldsymbol{x}. \end{aligned} \tag{3.8}$$

[6] How to match $\tilde{\mu}$ and μ is a question of ongoing research. Their quotient depends on the geometry of the porous medium [22]. We refer to [15, p. 27], [22, p. 13] and [23] for a more detailed discussion.

Note that $\boldsymbol{K}_\varepsilon^p$ has only positive entries. Since we aim at an upper estimate for the left hand side of this equation, we omit the last two positive terms on that side. In the next step, the proof proceeds with the application of the Cauchy-Schwarz and Poincaré's inequality just as in [3].

Furthermore, in order to derive estimate (3.6), the variational formulation of the difference $\boldsymbol{u}_{\varepsilon,\delta} - \boldsymbol{u}_\varepsilon$ has to be considered. As above, the same positivity argument for $\boldsymbol{K}_\varepsilon^p$ can be applied. □

Note that Theorem 3.1 is formulated for no-slip conditions on $\partial\Omega_\varepsilon$. Furthermore, it needs the interface conditions on Λ_ε to be sufficiently regular, i.e. the porous part is not allowed to touch the boundary. In contrast to that, textiles have a periodic structure and thus involve porous parts which might touch the boundary. But if we consider a slightly larger domain and extend the velocity by zero to its boundary, Theorem 3.1 still holds.

3.4. Computation of the microscale permeability. There remains the question how the permeability $\boldsymbol{K}_\varepsilon^p$ of the yarns is determined. We resort to two different methods:

(a) Follow the same approach as on the mesoscale in Section 2: In a microscale unit cell (Fig. 3.1, c), $\boldsymbol{K}_\varepsilon^p$ can be computed from the solution of the the unit cell problems.
(b) Employ a simplified computation of $\boldsymbol{K}_\varepsilon^p$ by semi-analytical formulas.

The latter approach may be used to avoid the complex numerical modelling of a further scale of the textile composite. Scanning electron microscopy shows that fibres are arranged in bundles having the shape of cylinders with ellipsoidal cross-sections [9]. Therefore, to compute the local permeability tensor $\boldsymbol{K}_\varepsilon^p$ of the yarns, the fibres in the yarns are locally approximated as a regular array of cylinders. Then, the components of $\boldsymbol{K}_\varepsilon^p$ can be calculated according to the semi-analytical formulas of Berdichevsky [8] and Gebart [9] by

$$\begin{aligned} K_\parallel &= \frac{R^2}{8V_f}\left[\ln\frac{1}{{V_f}^2} - (3 - V_f)(1 - V_f)\right] \\ K_\perp &= \frac{16}{9\pi\sqrt{2}}\left(\sqrt{\frac{V_{f\,\max}}{V_f}} - 1\right)^{\frac{5}{2}} R^2. \end{aligned} \tag{3.9}$$

Here, V_f denotes the local fibre volume fraction, R is the radius of the cylinders and $V_{f\,\max} = \pi/4$ is the maximum fibre volume fraction for a quadratic arrangement of cylinders. The formulas (3.9) give the permeability along ($K_\parallel$) and orthogonal ($K_\perp$) to the direction of the cylinder axis. Note that in realistic textiles, the yarns are not aligned with the unit cell axis. Then, an appropriate projection into the unit cell coordinate system is required.

Besides the local microscale yarn permeability $\boldsymbol{K}_\varepsilon^p$, we need to compute the macroscale permeability $\boldsymbol{K}$ as input for Darcy's law analogously to Section 2. Therefore, we have to consider the upscaling of the Stokes/Brinkman equations as done in [23]. This will be discussed in the following section.

3.5. Homogenisation of the Stokes/Brinkman equations. Similar to the homogenisation of the Stokes equations a formal asymptotic expansion (2.4) can be inserted into the Stokes/Brinkman equations (3.5). In [23] it is argued that if $\mu(\boldsymbol{K}_\varepsilon^p)^{-1} \geq \mathcal{O}(\varepsilon^{-2})$, the following Brinkman unit cell problem is obtained: For

$1 \leq i, j \leq 3$, find $(\boldsymbol{w}^i, \pi^i)$ such that

$$\begin{aligned} (\boldsymbol{K}_\varepsilon^p)^{-1}\boldsymbol{w}^i - \frac{\tilde{\mu}}{\mu}\Delta\boldsymbol{w}^i + \nabla\pi^i = \boldsymbol{e}^i \quad & \text{in } Y \\ \nabla\cdot\boldsymbol{w}^i = 0 \quad & \text{in } Y \\ \boldsymbol{w}^i, \pi^i \quad & Y-\text{periodic}, \end{aligned} \tag{3.10}$$

where $\boldsymbol{e}^i$ is the vector with components $e^i_j = \delta_{ij}$ and

$$K_{ij} = \langle w^i_j \rangle_Y .$$

In Ω, the upscaled flux is again given by Darcy's law

$$\begin{aligned} \boldsymbol{u} &= -\frac{\boldsymbol{K}}{\mu}(\nabla p - \boldsymbol{f}) \\ \nabla\cdot\boldsymbol{u} &= 0. \end{aligned} \tag{3.11}$$

For porous media with two pore scales, we now have an additional unit cell problem on the mesoscale (Fig. 3.1, b). This problem has to be solved for the computation of $\boldsymbol{K}$ for Darcy's law on the macroscale and requires as input the permeability $\boldsymbol{K}_\varepsilon^p$ of the microscale.

3.6. Numerical treatment of the Stokes/Brinkman equations. Altogether, we are now able to compute the permeability of geometries which embed porous obstacles Ω_ε^p. In these domains, we established the validity of the Stokes/Brinkman equations by Theorem 3.1. Its homogenisation requires the solution of the Brinkman unit cell problems. To this end, we gave two possibilities for the computation of the microscale permeability $\boldsymbol{K}_\varepsilon^p$. In the following, we numerically compare the solution of the Brinkman unit cell problems (3.10) on the mesoscale with the solution of the Stokes unit cell problems (2.8) on the microscale. Note that in the unit cell, these problems correspond to the solution of the Stokes/Brinkman equations and the Stokes equations, respectively, where both are driven by a unit force. Then, we compute the permeability of a real-life industrial textile.

Here, we again use our solver NaSt3DGP. Then, additionally to the diffusive term, the Brinkman term $\mu\boldsymbol{K}_\varepsilon^{-1}\boldsymbol{w}^i$, $i = 1, ..., 3$ has to be transported implicitly in time to avoid further time-step restrictions due to stability reasons. Again, the Crank-Nicolson scheme is employed, and the resulting linear system of equations is solved by the conjugate gradient method.

3.6.1. Test problem: 3D array of cubes. As a test case, we consider a fluid domain partially filled with cubes (Fig. 3.2). This geometry is a simple example of a unit cell from a dually porous medium.

On the microscale, where the geometry is resolved explicitly (cf. Fig. 3.1, b), we face the unit cell problems (2.8), i.e. we solve the Stokes equations both in the fluid and in the porous domain with periodic boundary conditions and unit force in x-direction for the computation of the permeability K_{11}. This direct numerical simulation of the flow requires a very fine - in general prohibitively fine - grid resolution. Instead, we can switch to the mesoscale and solve the Brinkman unit cell problems (3.10). Then, the porous geometry is no longer explicitly given (cf. Fig. 3.1, b), and we first have to compute the permeability $\mathbf{K}_\varepsilon^p$ of the porous part. This is done by method (a) in Subsection 3.4 and yields $K^p_{\varepsilon,11} = 1.73_{-1}$.[7] With this value, we solve

[7] In dimensionless calculations, the permeability $K_{\varepsilon,11} = 1.73_{-1}$ has to be rescaled by a factor of 0.0625^2, which is the squared length of one periodic cell of the geometry in Figure 3.2.

TABLE 3.1

Results from the computation of the unit cell problems (2.8) resolved on the microscale and from the Brinkman unit cell problems (3.10) resolved on successively refined grids on the mesoscale: Permeability and ratio of Brinkman term versus viscous term.

Problem	Resolution	K_{11}	$K^p_{\varepsilon,11}\Delta w_1/w_1$: min ... max
Stokes unit cell	$256 \times 256 \times 256$	5.43_{-2}	–
Brinkman unit cell	$032 \times 032 \times 032$	5.27_{-2}	3.3_{-6} ... 9.2_{-4}
	$064 \times 064 \times 064$	5.05_{-2}	5.3_{-7} ... 2.3_{-4}
	$128 \times 128 \times 128$	4.97_{-2}	1.2_{-7} ... 5.9_{-5}
	$256 \times 256 \times 256$	4.92_{-2}	2.8_{-8} ... 1.5_{-5}

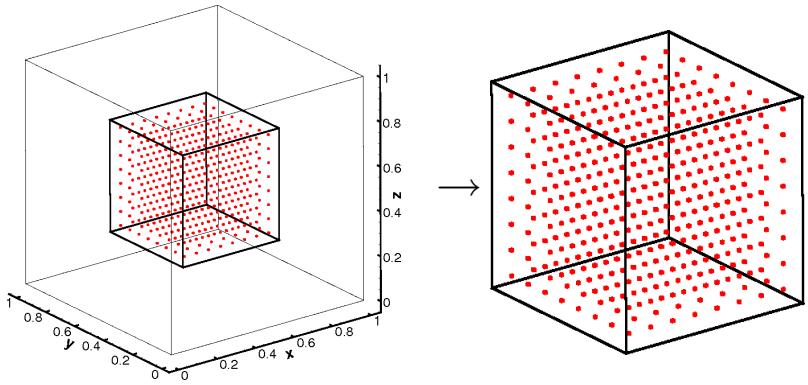

FIG. 3.2. *Test geometry: Domain filled partially with a porous medium consisting of cubes.*

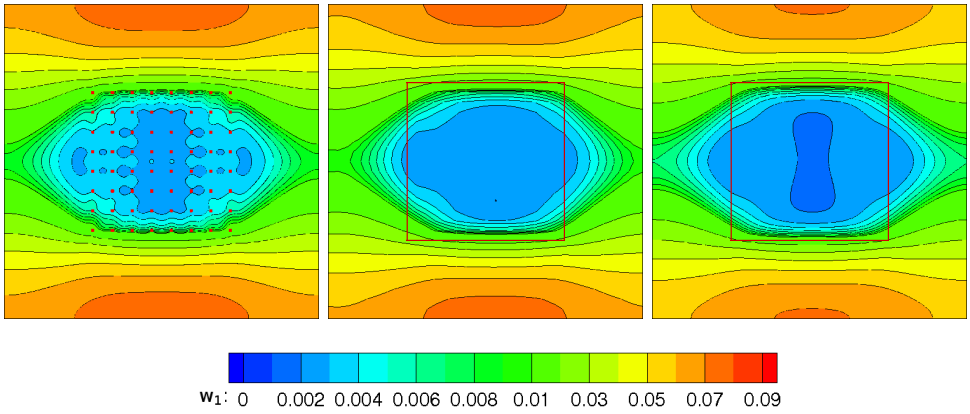

FIG. 3.3. *Results from the computation of the unit cell problems (2.8) resolved on the microscale and from the Brinkman unit cell problems (3.10) resolved on successively refined grids on the mesoscale. Drawn is a slice in the direction of the flow field from left to right. Compared are the contours of the velocity component w_1 in the microgeometry with a resolution of $256\times256\times256$ (left) and in the mesogeometry with a resolution of $32\times32\times32$ (middle) and a resolution of $128\times128\times128$ grid cells (right). The square denotes the porous part of the domain.*

TABLE 3.2
Convergence table for the solution of the Brinkman unit cell equations in a geometry filled partially with a porous medium.

$1/h$	$e^{w_1}_{h,1}$	$\rho^{w_1}_{h,1}$	$e^{w_1}_{h,\infty}$	$\rho^{w_1}_{h,\infty}$	$e^{w_2}_{h,1}$	$\rho^{w_2}_{h,1}$	$e^{w_2}_{h,\infty}$	$\rho^{w_2}_{h,\infty}$	$e^{\pi}_{h,1}$	$\rho^{\pi}_{h,1}$	$e^{\pi}_{h,\infty}$	$\rho^{\pi}_{h,\infty}$
32	3.538_{-3}	–	1.341_{-2}	–	5.110_{-4}	–	5.739_{-3}	–	2.863_{-2}	–	0.424	–
64	1.294_{-3}	1.451	6.058_{-3}	1.146	2.332_{-4}	1.132	2.965_{-3}	0.953	1.374_{-2}	1.060	0.294	0.530
128	5.068_{-4}	1.352	2.600_{-3}	1.221	1.021_{-4}	1.192	1.341_{-3}	1.145	6.048_{-3}	1.184	0.177	0.729

the Brinkman unit cell problems on four successively refined grids. The results are given in Table 3.1.

We observe convergence with successively finer grid resolution for the computation of permeability by the Brinkman unit cell problems. Note however that the permeability does not converge to that of the Stokes equations. This is due to the fact that the Stokes/Brinkman equations in the mesoscale unit cell are merely an approximation of the Stokes equations in the microscale unit cell, i.e. we always make a distinguishable error in solving them - instead of the microscopic problem directly.

Nevertheless, we observe that - even for a much coarser resolution - the Stokes equations are quite well approximated by the Stokes/Brinkman equations. This can be seen from the similarity in the flow fields depicted in Figure 3.3. This figure also shows that the oscillations of the flow field in the porous part on the microscale are averaged by the solution of the Brinkman unit cell equations on the mesoscale.

Let us recall that we have to justify the use of the Brinkman equation in a regime where Darcy's law was found to be valid in Section 2. In the case of the above porous medium filled partially with boxes, the Brinkman term $K_{11}^{-1}w_1$ dominates over the viscous term Δw_1, and hence, in the porous part, the Stokes/Brinkman equations reduce to Darcy's law. The ratio $K_{11}\Delta w_1/w_1$ of both terms is given in Table 3.1. As to be expected, this ratio is very low and varies between 3.3_{-6} and 9.2_{-4} on the coarsest grid. It even improves with a convergence rate of nearly $\mathcal{O}(h^2)$ on the finer grids.

In order to assess the quality of our numerical scheme, we compute the convergence rate for the solution of the Brinkman unit cell problem. Here, in contrast to Subsection 2.3.1, we employ the solution computed on the grid with mesh-width $1/256$ as reference solution Ψ_{ref}, where $\Psi \in \{w_1, w_2, \pi\}$. We define the error $e^{\Psi}_{h,p} = \|I^{\text{ref}}_h \Psi_h - \Psi_{\text{ref}}\|_{l^p_h}$ with $p \in \{1, \infty\}$, where I^{ref}_h denotes the interpolation of data computed on a mesh with mesh-width h to the reference mesh with mesh-width $1/256$. The convergence rate is then given by $\rho^{\Psi}_{h,p} = \ln\left(\frac{e^{\Psi}_{2h,p}}{e^{\Psi}_{h,p}}\right) / \ln 2$.[8] The resulting numbers are shown in Table 3.2.

We cannot expect full second order convergence because of the velocity jump of w_1 at the interface. This jump becomes manifest in steep gradients in the pressure near the interface as well as in the singular behaviour of the components w_2 and w_3 at the edges of the porous body. Accordingly, we find convergence rates near one for the velocities as well as for the pressure. Note that the results obtained for the velocities w_2 and w_3 are identical due to the symmetry of the problem. Similar to Subsection 2.3.1 we anticipate ρ to improve for a smaller size of the square porous

[8] Our solver NaSt3DGP employs a time stepping procedure, and we choose an explicit Euler scheme with $\delta t = 7.630_{-7}$ for the first time step. Then, time is discretised equidistantly by $\delta t = 2.289_{-4}$ for the implicit solver for all mesh-widths. We stop the simulation at time $t = 0.931$.

TABLE 3.3

Parameters of the non-crimp fabrics' unit cells and computational results with the Stokes (S) and Stokes/Brinkman (S/B) equations, i.e. results for impermeable and permeable yarns, respectively. The length of the unit cell $L = (L_x, L_y, L_z)$ is given in [mm] and K_{11} in [mm^2].

Preform name	L_x	L_y	L_z	Resolution	K_{11} S	K_{11} S/B
Bi-axial	3.4	4.92	0.45	$85 \times 123 \times 15$	2.73_{-4}	4.03_{-4}
Quadri-axial	8.195	5.06	0.945	$149 \times 92 \times 21$	5.21_{-4}	7.90_{-4}

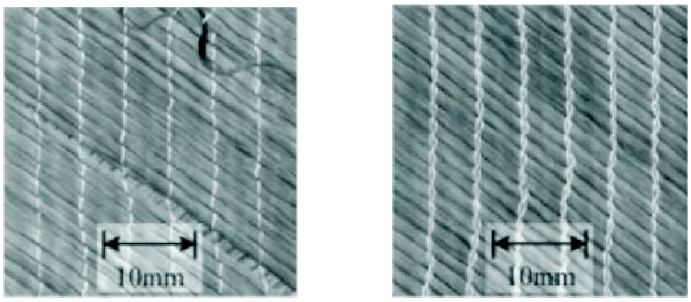

FIG. 3.4. *Bottom and top view on a non-crimp fabric with a chain stitch pattern; picture from [16].*

inclusion and therefore, for less interfaces at which the velocity is discontinuous.

In conclusion, the above results advocate the application of the Brinkman unit cell equations. This approach avoids the high resolution and long computing times that are needed for the solution on the microscale and leads to a sufficiently accurate and fast computation of permeability on the mesoscale instead. Note finally, that as long as the modeling error (3.6) of the Stokes/Brinkman equations is substantially below the mesh resolution, our approach is also numerically and analytically fully valid since the numerical error dominates anyway.

3.7. Non-Crimp Fabric. In this section we present experimental validation for non-crimp fabrics. These fabrics are widely used in the construction of composites such as wind blades, yachts, aircrafts and helmets. They consist of plies of aligned fibres which are stitched together with typical angles of 45° or 90°. The alignment of fibres and the stitching can be seen in Figure 3.4, where an example of a unidirectional non-crimp fabric is shown. Although the stitching yarns are one order of magnitude smaller than the fibre bundles they join, they have an important influence on the permeability since empty spaces are formed around the stitching. We consider two different types of non-crimp fabrics: a bi-axial and a quadri-axial fabric; see [17] for a more detailed description. Note that due to the structural properties of the textile, nesting can be neglected.

The non-crimp fabric has a very dense structure, so that intra-yarn flow becomes of particular importance. Therefore, we solve the Stokes/Brinkman equations (3.10) in the unit cell. Here, we resort to the semi-analytical formulas (3.9) for the computation of the microscale permeability $\boldsymbol{K}_\varepsilon^p$ as input for the Stokes/Brinkman equations. In order to assess the influence of intra-yarn flow and for comparison reasons, we additionally solve the Stokes equations for the computation of $\boldsymbol{K}$ as done in Section 2, i.e. we suppose that the yarns are impermeable.

The two numerical permeabilities are computed for a volume fraction of 38% for

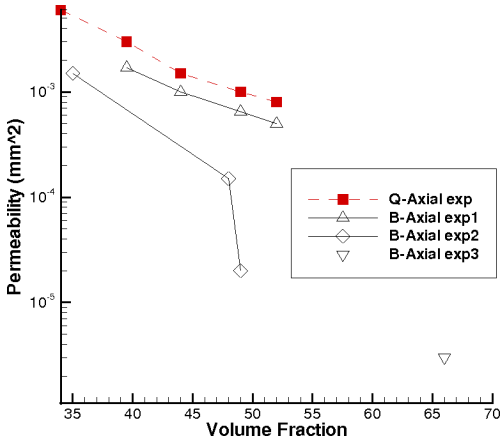

FIG. 3.5. *Results of four experiments on non-crimp fabrics.*

the bi-axial and of 40% for the quadri-axial non-crimp fabric. In Table 3.3, we see a comparison between the permeability computed in the case that intra-yarn flow is taken into account (the Stokes/Brinkman equations are solved) and in the case that the yarns are treated as impermeable (the Stokes equations are solved). As expected, the permeability is considerably lower in the latter case.

Next, to validate our numerical results we refer to measurements obtained from practical experiments. These were performed by the TECABS consortium (EPFL, Ecole des Mines de Douai, K.U. Leuven, 2004). For detailed information about the bi-axial and quadri-axial non-crimp fabrics, see Appendix D of [28]. Figure 3.5 gives the available numbers. We clearly see a decrease of the permeability with increasing volume fraction. We furthermore observe from the two bi-axial experiments that there is quite a variability in the measured permeability. This is due to the fact that the experimental setup is difficult, i.e. the measurement error is in the range of 10^{-4}. In comparison, the results of our numerical experiments are approximately in the same range. For the quadri-axial fabric with a volume fraction of 40%, we obtained a value of $7.90_{-4}\,\mathrm{mm}^2$, and for the bi-axial fabric with a volume fraction of 38 %, we obtained a value of $4.03_{-4}\,\mathrm{mm}^2$. Nevertheless, the numerically computed permeability underestimates the experimental values. However, the results clearly improve by the application of the Stokes/Brinkman equations for intra-yarn flow.

4. Concluding remarks. In this paper we presented a numerical multiscale method for the computation of permeability of industrial textiles in three dimensions.

First, we considered the case of impermeable textile yarns. Here, we justified Darcy's law on the textile macroscale by homogenisation theory. In particular, we showed that the computation of permeability defined by the solution of the unit cell problems is indeed equivalent to its computation by Darcy's law. Our numerical scheme employs a staggered grid with a finite difference discretisation and a projection method. We solved the unit cell problems as well as the Stokes equations and Darcy's law for the permeability. For a simple test problem our results agreed well with semi-analytical values from the literature [26]. Furthermore, we computed the permeability of the industrial textile Monofilament Fabric Natte 2115 and obtained values which were very close to those measured in practical experiments.

In a second step, we considered the case of permeable textile yarns. To this end,

we discussed the validity of the Stokes/Brinkman equations which account for the dual porosity of textiles. Again, homogenisation yields Darcy's law on the macroscale. We employed our numerical scheme for the solution of the Stokes/Brinkman unit cell equations. For a test problem, their solution compares very well with the direct numerical solution of the Stokes equations on the microscale. Furthermore, we numerically showed the reduction of the Stokes/Brinkman equations to Darcy's law in the porous domain. The presented method was then applied to non-crimp fabrics with permeable yarns. There, our numerically computed permeability also agreed sufficiently well with available experimental data.

Acknowledgements. The authors acknowledge the support from the Sonderforschungsbereich 611 "Singular Phenomena and Scaling in Mathematical Models" of the Deutsche Forschungsgemeinschaft DFG.

We are grateful to Prof. D. Roose, Prof. S. V. Lomov and Dr. B. Verleye of the Department of Computer Sciences of the K.U. Leuven for providing the textile geometries and we thank them for the fruitful discussions on the computation of textile permeability.

REFERENCES

[1] G. Allaire. Homogenization of the Stokes flow in a connected porous medium. *Asymptotic Analysis*, 2:203–222, 1989.

[2] G. Allaire. Homogenization of the Navier-Stokes equations and derivation of Brinkman's law. *Applied Mathematics for Engineering Sciences*, pages 7–20, 1991.

[3] P. Angot. Analysis of singular perturbations on the Brinkman problem for fictitious domain models of viscous flow. *Mathematical Methods in the Applied Sciences*, 22(16):1395–1412, 1999.

[4] P. Angot, C.H. Bruneau, and P. Fabrie. A penalization method to take into account obstacles in incompressible viscous flows. *Numerische Mathematik*, 81(4):497–520, 1999.

[5] G.S. Beavers and D.D. Joseph. Boundary conditions at a naturally permeable wall. *Journal of Fluid Mechanics*, 30:197–207, 1967.

[6] M. Belhadj, E. Cancès J.F. Gerbeau, and A. Mikelic. Homogenization approach to filtration through a fibrous medium. *Networks and Heterogeneous Media*, 2(3):529–550, 2007.

[7] A.Yu. Beliaev and S.M. Kozlov. Darcy equation for random porous media. *Communications on Pure and Applied Mathematics*, 49(1):1–34, 1996.

[8] A.L. Berdichevsky and Z. Cai. Preform permeability predictions by self-consistent method and finite element simulation. *Polymer Composites*, 14(2):132–143, 2004.

[9] B.R. Gebart. Permeability of unidirectional reinforcements for RTM. *Journal of Composite Materials*, 26(8):1100–33, 1992.

[10] M. Griebel, T. Dornseifer, and T. Neunhoeffer. *Numerical Simulation in Fluid Dynamics, a Practical Introduction*. SIAM, Philadelphia, 1998.

[11] K. Hoes. *Development of a New Sensor-Based Setup for Experimental Permeability Identification of Fibrous Media*. PhD thesis, Vrije Universiteit Brussel, 2003.

[12] K. Hoes, D. Dinesku, M. Vanhuele, H. Sol, R.S. Parnas, E.B. Belov, and S.V. Lomov. Statistical distribution of permeability values of different porous materials. In H. Sol and J. Degrieck, editors, *10th European Conference on Composite Materials (ECCM-10)*, 2001.

[13] U. Hornung. *Homogenization and Porous Media*. Interdisciplinary Applied Mathematics Volume 6, Springer-Verlag, New York, 1996.

[14] M. Klitz. Homogenised Fluid Flow Equations in Porous Media with Application to Permeability Computations in Textiles. Diplomarbeit, Institut für Numerische Simulation, Universität Bonn, July 2006.

[15] V. Laptev. *Numerical Solution of Coupled Flow in Plain and Porous Media*. PhD thesis, Universität Kaiserslautern, 2003.

[16] R. Loendersloot. *The structure-permeability relation of textile reinforcements*. PhD thesis, Universiteit Twente, 2006.

[17] S.V. Lomov, E.B. Belov, T. Bischoff, S.B. Ghosh, T.C. Truong, and I. Verpoest. Carbon composites based on multiaxial multiply stitched preforms. Part 1: Geometry of the preform. *Composites Part A*, 33(9):1171–1183, 2002.

[18] S.V. Lomov, I. Verpoest, T. Peeters, D. Roose, and M. Zako. Nesting in textile laminates: geometrical modelling of the laminate. *Composites Science and Technology*, 63(7):993–1007, 2002.

[19] C.C. Mei, J.L. Auriault, and C.O. Ng. Some applications of the homogenization theory. *Advances in Applied Mechanics*, pages 277–348, 1996.

[20] A. Mikelic. *Homogenization Theory and Applications to Filtration through Porous Media*, volume 1734/2000 of *Lecture Notes in Mathematics*, pages 127–214. Springer, Berlin, Heidelberg, 2000.

[21] P.B. Nedanov and S.G. Advani. Numerical computation of the fiber preform permeability tensor by the homogenization method. *Polymer composites*, 23(5):758–770, 2002.

[22] D.A. Nield and A. Bejan. *Convection in Porous Media*. Springer-Verlag New York, 2nd edition, 1999.

[23] P. Popov, Y. Efendiev, and G. Qin. Multiscale modeling and simulations of flows in naturally fractured karst reservoirs. *Commun. Comput. Phys.*, 6:162–184, 2009.

[24] S. Rief. *Numerical Solution of the Navier-Stokes System with Two Pressures and Application to Paper Making*. PhD thesis, Universität Kaiserslautern, 2005.

[25] R. Sanchez-Palencia. *Non-Homogeneous Media and Vibration Theory*. Lecture Notes in Physics 127. Springer-Verlag, Berlin, 1980.

[26] A.S. Sangani and A. Acrivos. Slow flow through a periodic array of spheres. *International Journal of Multiphase Flow*, 8(4):343–360, 1982.

[27] L. Tartar. *Incompressible Fluid Flow in a Porous Medium - Convergence of the Homogenization Process*, pages 368–377. Appendix of: Lecture Notes in Physics 127. Springer-Verlag, Berlin, 1980.

[28] B. Verleye. *Computation of the permeability of multi-scale porous media with application to technical textiles*. PhD thesis, Katholieke Universiteit Leuven, 2008.

[29] B. Verleye, R. Croce, M. Griebel, M. Klitz, S.V. Lomov, G. Morren, H. Sol, I. Verpoest, and D. Roose. Permeability of textile reinforcements: Simulation, influence of shear and validation. *Composites Science and Technology*, 68(13):2804–2810, 2008.

[30] B. Verleye, S.V. Lomov, A.C. Long, I. Verpoest, and D. Roose. Permeability prediction for the meso-macro coupling in the simulation of the impregnation stage of resin transfer moulding. *Composites Part A*, 2009. In print.

[31] I. Verpoest and S.V. Lomov. Virtual textile composites software WiseTex: integration with micro-mechanical, permeability and structural analysis. *Composites Science and Technology*, 65(15-16):2563–2574, 2005.